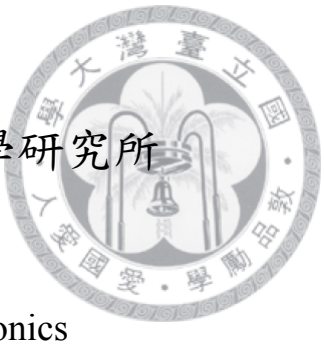

國立臺灣大學電機資訊學院光電工程學研究所

碩士論文

Graduate Institute of Photonics and Optoelectronics
College of Electrical Engineering and Computer Science
National Taiwan University

Master Thesis

以結合微流道之銦鎵鋅氧化物薄膜電晶體偵測蛋白質與配體之反應行為

Integration of Microfluidic Channels with IGZO Thin Film Transistors for Detecting Protein-Ligand Interactions

吳守浩

Shou-Hao Wu

指導教授：馮哲川 博士 / 黃建璋 博士

Advisor: Zhe Chuan Feng, Ph.D. / JianJang Huang, Ph.D.

中華民國 一o三 年 七 月

July 2014

國立臺灣大學碩士學位論文
口試委員會審定書

以結合微流道之銦鎵鋅氧化物薄膜電晶體
偵測蛋白質與配體之反應行為
Integration of Microfluidic Channels with
IGZO Thin Film Transistors for
Detecting Protein-Ligand Interactions

本論文係吳守浩君（學號 R01941053）在國立臺灣大學光電工程學研究所完成之碩士學位論文，於民國 103 年 7 月 24 日承下列考試委員審查通過及口試及格，特此證明

口試委員：

馮哲川　（指導教授）

楊宗霖　吳育任

黃建璋

所　長　林恭如

謝誌

謝謝馮哲川與黃建璋老師的指導。老師時常展現快速又充滿創意的思考。跟隨老師的指導做研究常常會在驚奇和趣味之中同時學習到許多知識以及做事的方法。謝謝 TFT 組裡面的老蘇學長、黃凱學長、嘉璟學姊還有正在博班路上奮鬥的煜峰學長，在半導體製程和進階的量測技術給予我相當充分的訓練。除了實驗之外，向學長姊們討論產業界或生涯規劃等資訊也使我獲益良多。感謝怡文總是這麼可靠地提供各種幫助。若沒有怡文的支援，我的研究肯定會進行得更加辛苦艱難。謝謝我的好戰友們，果凍、阿鴻、祥瑋、柏豪、韋諭。能跟你們進同一間實驗室實在很幸運。大家都知道怎麼認真也知道怎麼玩，讓我在辛苦的日子裡負擔減半、在歡笑的時光中快樂加倍。當然也要謝謝晏翔、致皓、鎮宇、宗翰、挺瑒、昕逸、文翊這些日子的照顧，祝你們接下來的研究生活一切順利。By the way，meeting 煮點心實在太溫馨了，有時間的話希望能繼續保持。

最後感謝爸、媽、姊，我的女友和所有親戚朋友。謝謝你們無盡的支持與鼓勵，伴隨我走過一階段又一階段的挑戰，並賜予我力量，面對接下來的人生。

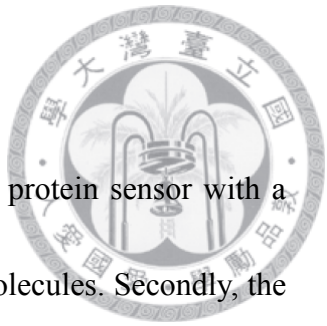

Abstract

There are two parts in this thesis. First of all, a TFT-based protein sensor with a microfluidic channel is designed to detect and quantify the bio-molecules. Secondly, the TFT sensor is further applied to detect the protein-ligand interaction between MDH and NADH.

We demonstrate a TFT-based protein sensor combined with microfluidic channel. Due to the concentration gradient in solution, the analyte diffuses to the sensing pad through the microfluidic channel and causes a drain current increment. With various microfluidic channel lengths or different concentrations of IgG antibody, the results of response (diffusion) time and the amount of induced charges are quite distinguishable. All results following some theoretical relations. Thus, the unknown concentrations of IgG antibody can be obtained. Our design can acquire not only electrical information (the charges carried by the bio-molecules) but also fluidic information (diffusion time which is related to the size and weight of the bio-molecules).

We next examine the diffusion and electrical signals of protein, ligand, and protein-ligand interaction. They were first measured separately to obtain information that would be referenced for later experiment. An estimation equation is provided for new analyte with unknown diffusion coefficient, and is verified in our experiment to have accurate evaluation of diffusion time. We also did the fluorescent snapshots to gain a visual picture

of the diffusion scheme aside from electrical measurement. Finally, protein-ligand interaction is detected by our TFT sensor.

Key words: a-IGZO, TFT, protein sensor, microfluidic channel, protein-ligand interaction

摘要

論文中包含了兩個部分。首先是將薄膜電晶體應用於血清蛋白的偵測，其次是其在偵測蛋白質與配體之間的反應行為。

生物分子的偵測是當今熱門的研究。我們設計的蛋白質感測器結合了微流道系統。當待測物經由微流道擴散到金感測板時，會造成薄膜電晶體電流瞬間增加。不同的流道長度或是蛋白質濃度，都會影響電流變化的時間以及感應電荷的數量。而這些結果又可以經由理論關係式相互推導，因而達到偵測與量化的目的。我們的設計可以得到電性方面的資訊(蛋白質帶電量)，並且同時可以得到流體的訊息(和蛋白質的尺寸大小及質量相關)，是一個非常簡易卻又方便迅速的蛋白質感測器。

另外，蛋白質與配體間的交互作用一直是世界各大藥廠相當關切的議題。我們首先用薄膜電晶體感測器偵測蛋白質與配體分別的訊號，並給出一個估算式以預估量測未知擴散係數的生物分子時適合的調配濃度。我們進行螢光染色的影像拍攝以驗證先前純粹電性量測的結果。最後我們將配體引入蛋白質溶液並量測其電性反應，以探究兩者之間的反應行為。

關鍵字：非晶相銦鎵鋅氧化物，薄膜電晶體，生物感測器，微流道，蛋白質配體反應行為

Table of Contents

List of Figures

List of Tables

Chapter 1 Introduction

1.1 Background of protein bio-sensor

1.1.1 Overview of protein detection

Biomedical engineering is a popular research topic nowadays. Cancer diagnostics and detection are the central investigating issue since cancer has been the top of the ten leading causes of death for over thirty years. Therefore the interest in human genes is significantly increasing and the investigations of bio-molecules (e.g. antibodies, nucleotides and peptides, etc.) are of great value in biological science [1, 2]. Protein molecules, in particular, has received considerable attention since the occurrence of diseases has appeared at the protein level [3, 4].

Traditional ways of diagnostics include blood tests, urinalysis and tumor markers. However, identification and quantification can be very complicated, time consuming and expensive. Thus, there is a rising need for convenient methods for detecting and measuring the levels of specific proteins.

There are existing techniques for the detection of proteins such as optical, mass spectrometry, and electrochemical measurements. Colorimetric protein assay (including BCA protein assay, Bradford assay, the Lowry method, etc.) [5] is one of the most common methods of protein measurement. The process is fast, simple and direct. However, the detection is nonspecific and inaccurate. In the meanwhile, Western blotting

[6] is a way commonly used to specifically detect the protein concentration as well as other methods such as spectrophotometric assay [7] and surface plasmon resonance (SPR) [8], but the sensitivity is limited and the process is sophisticated and time-consuming.

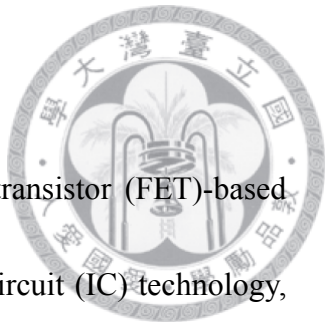

1.1.2 FET-based biosensors

To overcome the above mentioned problems, field effect transistor (FET)-based biosensors, which are widely used in semiconductor integrated circuit (IC) technology, have attracted a great deal of attention because of their various advantages in terms of miniaturization, standardization, mass-production. Especially, they are suitable for the on-chip integration of both the sensor and measurement systems [9, 10]. Comparing to traditional quantification methods, the required sample and detecting time are quite low.

The structure investigated most is nanorod transistor-based biosensor. The channel is replaced by the nanorods as illustrated in Fig 1.4 [11]. The material of the channel may be carbon nanotube, silicon nanowire, ZnO nanorods and so on. Since proteins are intrinsically charged, they can influence the carrier in the channel and lead to a change in drain current. Therefore, by monitoring drain current, the concentration of the proteins is revealed. The signal of protein detection process is illustrated in Fig 1.5 [11]. The structure suffers from difficulties in fabrication such as the alignment of nano-structure. Also the sensing area is small, basically the size of the semiconductor channel.

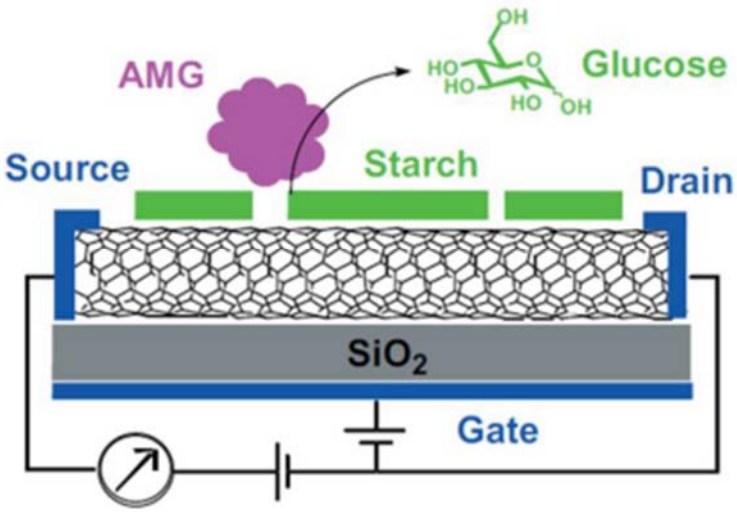

Fig 1.1. Demonstration of nanorods transistor-based biosensor. The channel is formed by the nanorods instead of the bulk and used as the sensing area. [11]

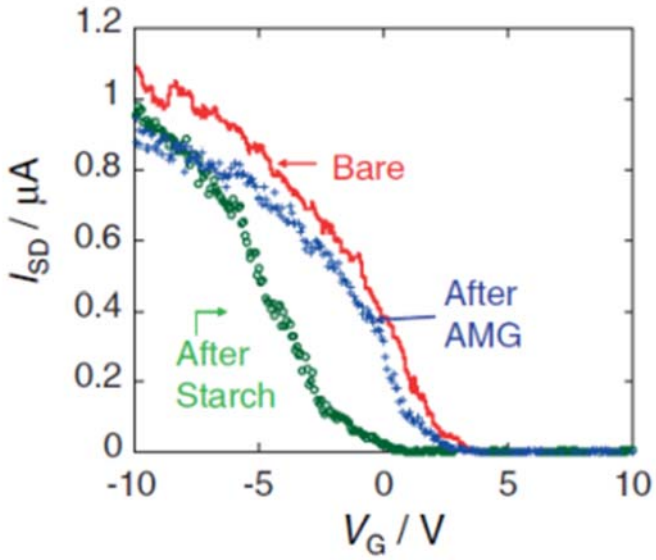

Fig 1.2. Illustration of signal of protein detection process. As the protein applying to the device, the drain current of the device switch to another level [11].

A problem might occur because of the poor isolation between the device and the biological solution. Thus, it is very important to develop an encapsulation process of biosensors that is compatible with the IC technology. Accordingly, most frequently used FET-type biosensor is an extended gate field effect transistor (EGFET) [12, 13]. Its structure (see Fig 1.6 [14]) brings about the isolation of transistor from the chemical or biological environment, in which a sensitive membrane is deposited on the end of a signal line extended from the transistor gate electrode. For such reasons, the EGFET structure has several advantages, such as insensitivity to temperature and light, simple method of passivation and packaging, flexibility of shape of the extended gate. Thus, it could be tested and characterized without the need for coming into contact with solutions [13].

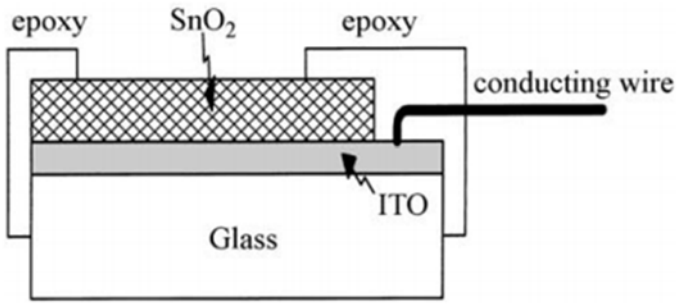

Fig 1.3 Cross section of an EGFET bio-sensor [14]

Therefore, we introduce a thin-film-transistor with extended sensing gold pads and a microfluidic channel that is designed to detect both the electronic and fluidic properties of proteins. The extended metal pad is designed for sensing the induced charge on the pad and also to avoid the biological solution contact with the IGZO TFT. On the other hand, the microfluidic channel is composed to get more information such as diffusion time from the biological solution through diffusion process in the microfluidic channel.

Chapter 2 TFT-based Protein Sensor with Microfluidic Channels

2.1 Introduction

2.1.1 Overview of the microfluidic system

The concept of microfluidics and lab-on-a-chip (LOC) was put forth by Widmer and Manz in 1990 [15] and is widely applied in chemical and biological analysis, such as the preparation and separation of molecules, monitoring, specific detection, quantification on a single device, etc. All these applications can be integrated with electronic or optical signal, making the concept of LOC more attractive.

The simplest microfluidic network design includes a set of orthogonally intersecting microchannels (see Fig 2.1 [16]). These channels provide for the controlled handling of small volume of aqueous analyte solution. Generally, the shorter channel functions as the injection unit while the longer channel usually provides the necessary conditions to facilitate separation of the mixture in the analyte solutions by electroosmosis or electrophoresis [17]. In principle, the detection units are integrated with the longer microchannel.

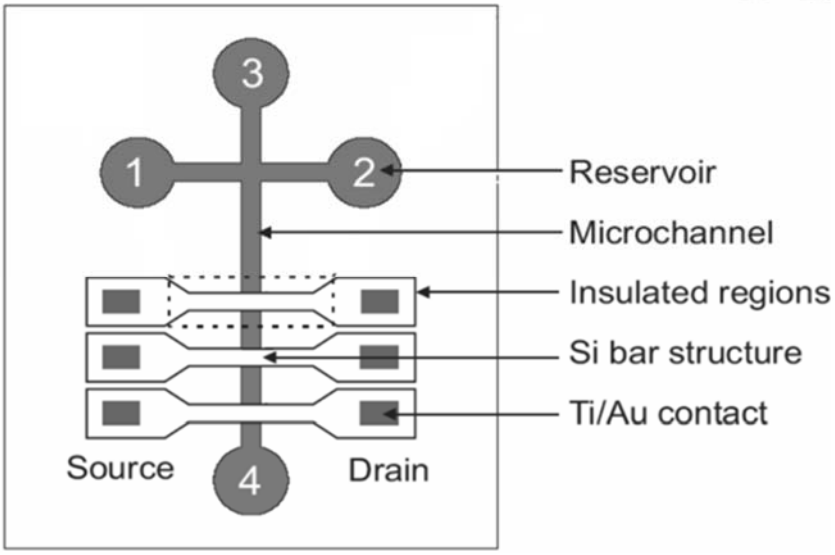

Fig 2.1. The structure of microfluidic network includes a set of orthogonally intersecting microchannels and some detectors. [16]

There is an enormous development in separation mode [18], detection schemes, analysis of biological species [19], biological and chemical reactors [20]. Thus, fabrication of microchannel has become more important. Polymer substrates are widely used due to their simple fabrication process (molding techniques), optical properties (transparency) and low cost. On the other hand, semiconductor substrates, particularly silicon, have gained an increasingly interest [21, 22] because their the direct integration of electronic components are becoming more and more feasible.

In recent years, numerous reports are suggesting that biosensors should be integrated with a microfluidic system for detection accuracy, sample volume reduction, fast response time and ultimately portable, disposable chip [23]. Most of the research use microfluidic channel just as a way to deliver the biological or chemical solution(see Fig 2.2 [1]). A few

reports combine these two methods and detect the optical signal progressing with time [24]. It means that only a little part of the ability of microfluidic system has been exploited to combine with the biosensors.

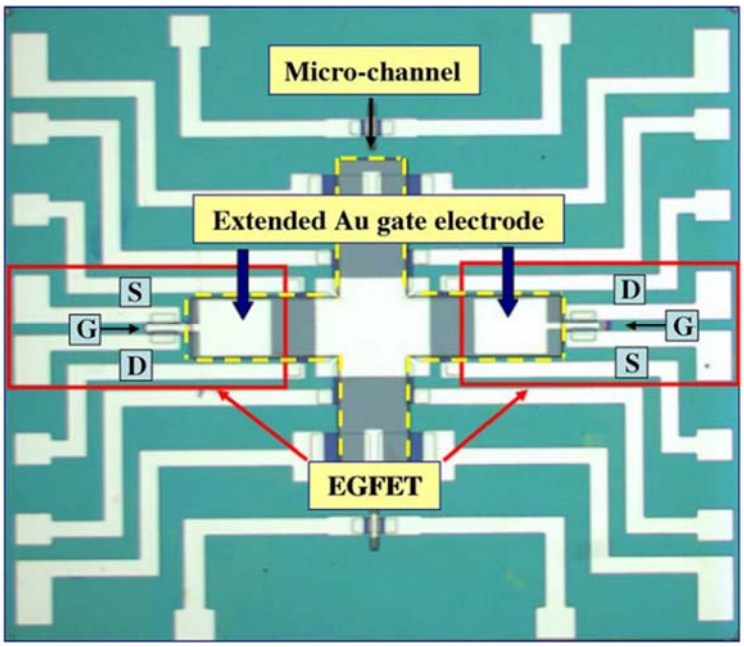

Fig 2.2 Micro-channel is used for delivering the solutions [1].

Therefore, we design a TFT-based biosensor with microfluidic channel to detect both electronic and fluidic properties of the analyte solution. There is a sensing gold pad extended from IGZO TFT and is designed for sensing the induced charge on the pad and also to avoid the biological solution contact with the device. On the other hand, the microfluidic channel is composed to get information from the biological solution while the analyte solutions diffuse in the microfluidic channel because of the created concentration gradient.

2.1.2 Introduction of the IgG antibody

Immunoglobulin G (IgG) antibody was used to charge the extended sensing pad. IgG antibodies, a major effector molecule of the humeral immune response in man, accounts for about 75% of the total immunoglobulin in plasma of healthy individuals.

IgG antibodies are very important in fighting bacterial and viral infections. They are large molecules, having a molecular weight of approximately 150 kDa, composed of two different kinds of polypeptide chain. One is heavy chain of approximately 50 kDa. And the other is termed light chain, and is about 25 kDa.

Each IgG antibody consists of two heavy chains and two light chains to form "Y" shape. For any IgG antibody, the two heavy chains and the two light chains are identical to recognize specific molecule, and thus they have the ability to bind simultaneously to identical structures [25].

2.1.3 Structure and mechanism

We design a protein detecting biosensor using IGZO TFT with extended sensing metal pad and microfluidic channel. The extended metal pad is designed for sensing the induced charge on the pad and also to avoid the biological solution contact with the TFT. On the other hand, the microfluidic channel is composed to observe the diffusion phenomenon when biological solution go through the microchannel.

As in Fig 2.3, there are mainly two parts in the device. One is the thin film transistor and the other is the extended sensing gold pad with patterned sink and microfluidic channel. The sensing gold pad is extended from the top of the IGZO channel of TFT with SiO_2 passivation layer in between. The patterned sink and microfluidic channel are formed by SU-8 which has a large depth to width ratio and can isolates the TFT from the biological solution.

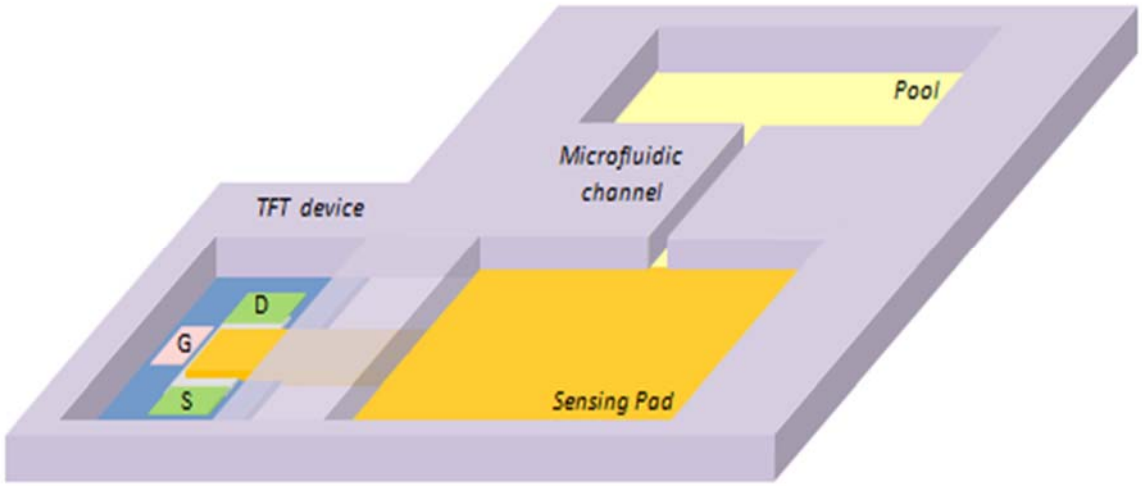

Fig 2.3. Structure of TFT-based biosensor with microfluidic channel

When a biological concentration gradient was created in the microfluidic channel, proteins may diffuse from regions of high concentration to regions of low concentration. By the law of diffusion, the concentration of protein affects the flux and the diffusion time.

Besides, most biological substances carry a few negative charges. Therefore, as they reach the sensing pad through diffusion, the sensing pad will be charged. By the Gauss's law, that may influence the carriers in the IGZO channel and thus change the drain current. The flux of the protein affects the amount of induced charge of the extended sensing pad and the drain current.

Consequently, the concentration of the protein can be measured through the variation of the drain current, the amount of induced charge amount and the protein diffusion time.

2.2 Device fabrication and measurement

2.2.1 Fabrication

The fabrication process is shown in Fig 2.4. A staggered and bottom gate configuration is employed to fabricate a-IGZO TFTs on Corning Eagle 2000 glass substrate. The process starts from molybdenum (Mo) gate metal by DC sputtering and reactive ion etching (RIE). Then a 80nm-thick SiO_2 dielectric layer is deposited by plasma enhanced chemical vapor deposition (PECVD) at 350℃. In the subsequent step, a 50nm IGZO film is coated by RF sputtering at room temperature. Next, the channel mesa is patterned by photolithography and dipping into dilute HCl for several seconds. Mo metal is coated by DC sputtering and etched by RIE, forming source and drain contacts. To eliminate the defects on the surface of IGZO caused by RIE, we dip the samples into dilute HCl again for a few seconds. Then we deposit 100nm SiO_2 passivation layer by RF sputtering at room temperature, which serves the purpose of protecting the devices and also as an insulator for the sensing metal pad. The via-holes are opened by RIE to expose the contact pads.

After the fabrication of the TFT, the sensing gold pad is evaporated by E-gun evaporation for 300nm, pattern defined by lift-off. Then we perform post-annealing at 300℃ under nitrogen ambient for an hour in an oven tube. Gold was selected as the material of the sensing pad since there have been studies showing that gold are of good

biocompatibility and are widely used in biomedical research.

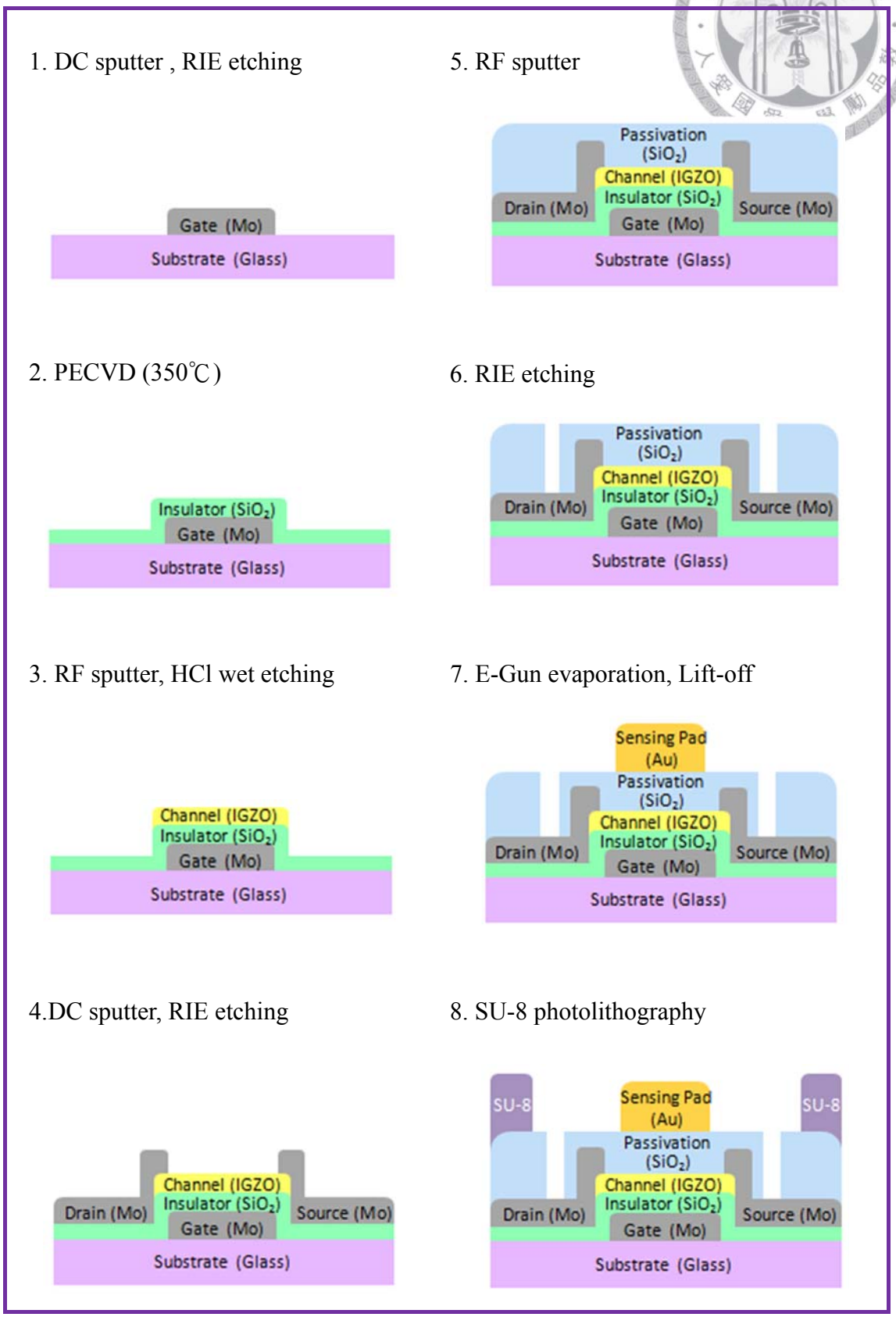

Fig 2.4. Fabrication process

Finally, SU-8 2100 was coated and patterned by photolithography to be the micro-sink and microfluidic channel of the bio-solution. SU-8 is a high contrast, epoxy based photoresist designed for micromachining. It has been designed as a permanent, high cross linked epoxy material and with high depth to width ratio. The fabrication process of patterned SU-8 is critical and need to be well controlled. The process flow of the fabrication of SU-8 is shown in Fig 2.5. The height of SU-8 is about 100μm.

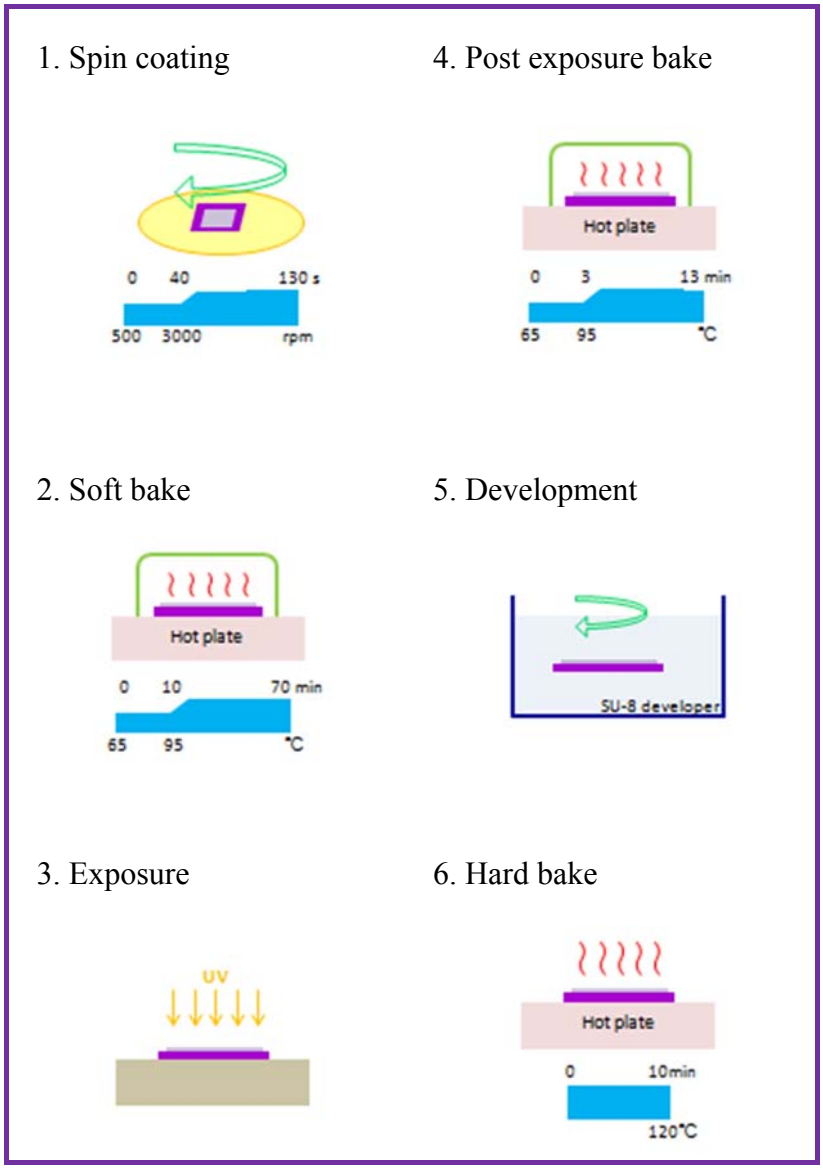

Fig 2.5 Fabrication of 100 μm SU8-2100

2.2.2 Method of measurement

As shown in Fig 2.6, the sensing pad and the microfluidic channel are first filled with phosphate buffered saline (PBS) before applying IgG antibody solution to the pool. The IgG antibody was purchased from Abcam Company in liquid form. It was diluted by 30, 50, and 100 times with PBS before the measurement.

The IgG antibody solution was then gradually diffused from the pool to the sensing pad through the microfluidic channel because of the concentration gradient. We start to see the change of TFT drain current as soon as the IgG antibody diffuses and conjugates with the sensing pad. It usually takes several minutes.

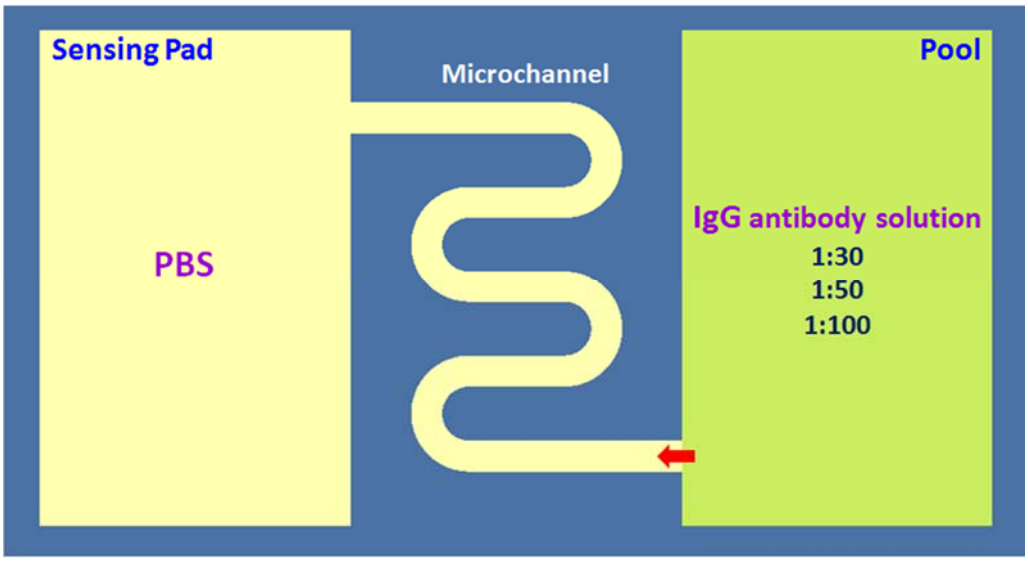

Fig 2.6 Solution condition before measurement.

2.3 Characterizations of TFT-based protein sensors

2.3.1 Drain current variations in time domain

The electrical properties of the TFTs were extracted by Agilent 4155C semiconductor parameter analyzer at room temperature. The IGZO channel width is 600 μm and length is 250 μm. We first measured the drain current of the devices with IgG antibody solution (IgG antibody : PBS = 1:50) and dispersed at the bias condition V_{GS} = 8 V and V_{DS} = 5 V. The measurement was repeated every 30 seconds.

For the samples with a microfluidic channel length of 2700 μm, the drain current is abruptly increased from 195.8 to 206.1 μA at 6.5 minute (see Fig 2.7), which implies that at t = 6.5 minute, the antibody reaches the sensing pad and conjugates with it, leading to the increment of drain current. Since IgG antibody carries some negative charges, they can be attached to the gold pad through Van der Waals force.

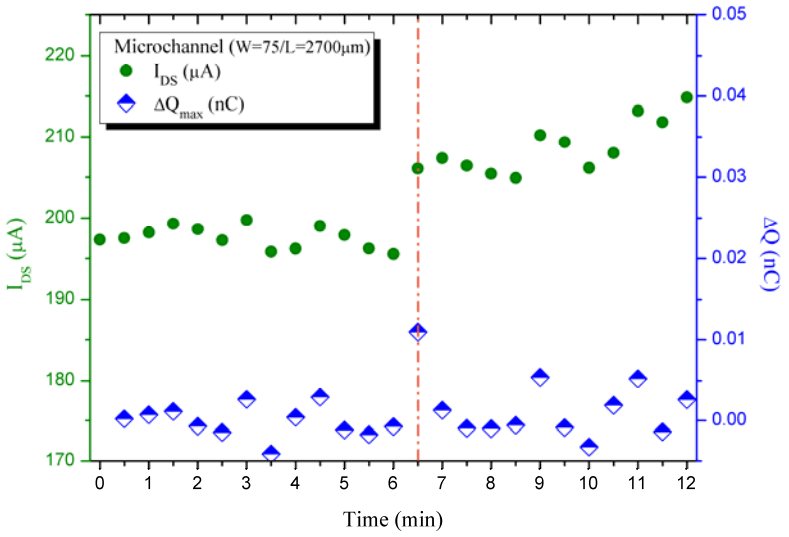

Fig 2.7. (channel length 2700 μm) Drain current and induced charge variation

To understand the change of I_{DS}-V_{DS} curves, Fig 2.8 show the transfer and modulation curves of the device before (t = 0) and after (t = 15 min) applying the IgG antibody solution. At V_{GS} = 8 V and V_{DS} = 5 V, the drain current is 180.4 at t=0, and increases to 228.7 μA at t = 15 minute. From the transfer curves, the application of IgG antibody result in little changes of threshold voltage as well as the subthreshold swing of the devices, indicating that the channel property remains nearly the same after the protein binding.

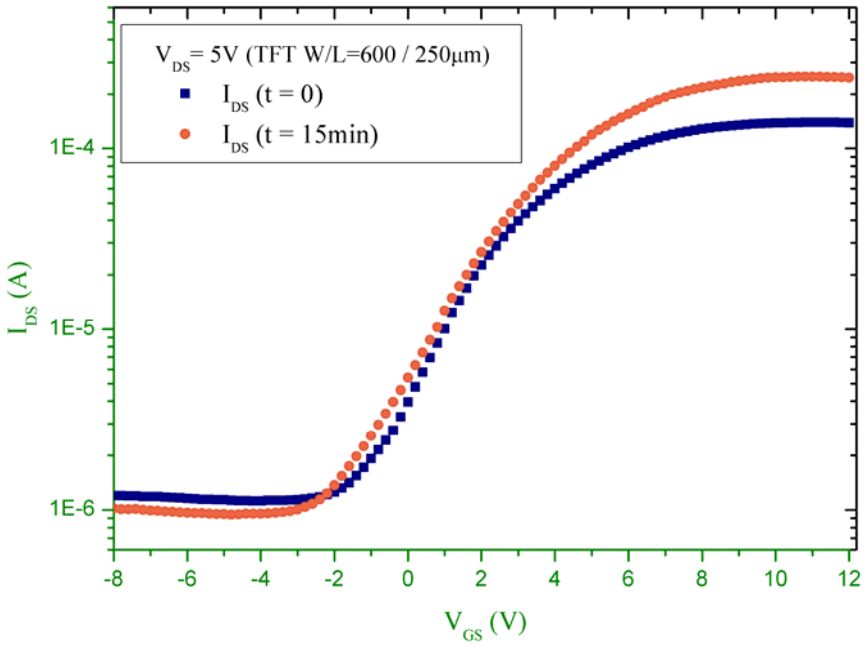

(a)

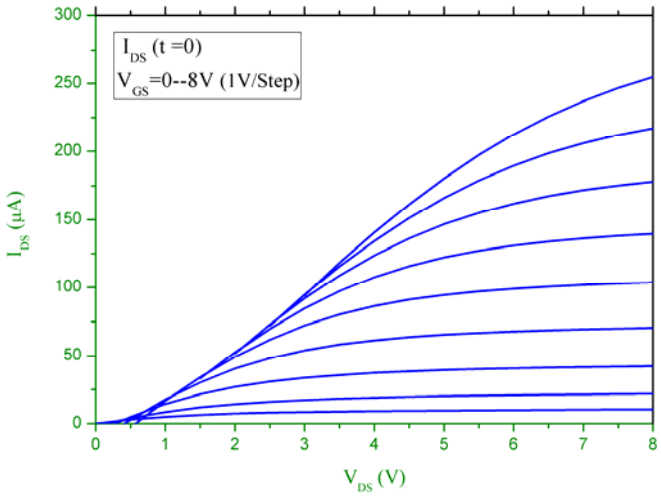

(b)

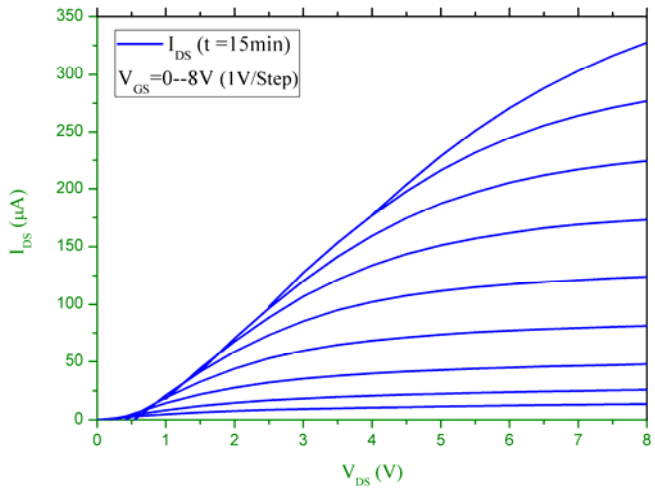

(c)

Fig 2.8 Properties of a-IGZO TFT (a) I_{DS}-V_{GS} at t = 0 and 15 min

(b) I_{DS}-V_{DS} at t = 0 (c) I_{DS}-V_{DS} at t = 15 min

We next measured the drain current on the sample with a shorter 1800 μm microchannel length. At t = 3 min, an abrupt increase of current from 350.5 to 383.6μA (see Fig 2.9) indicates that the antibody has reached the sensing pad. By comparing Fig 2.7 and 2.9, it is observed that the response time of drain current is dependent on the microfluidic channel length. With longer microchannel length (2700 μm) , the response time is later.

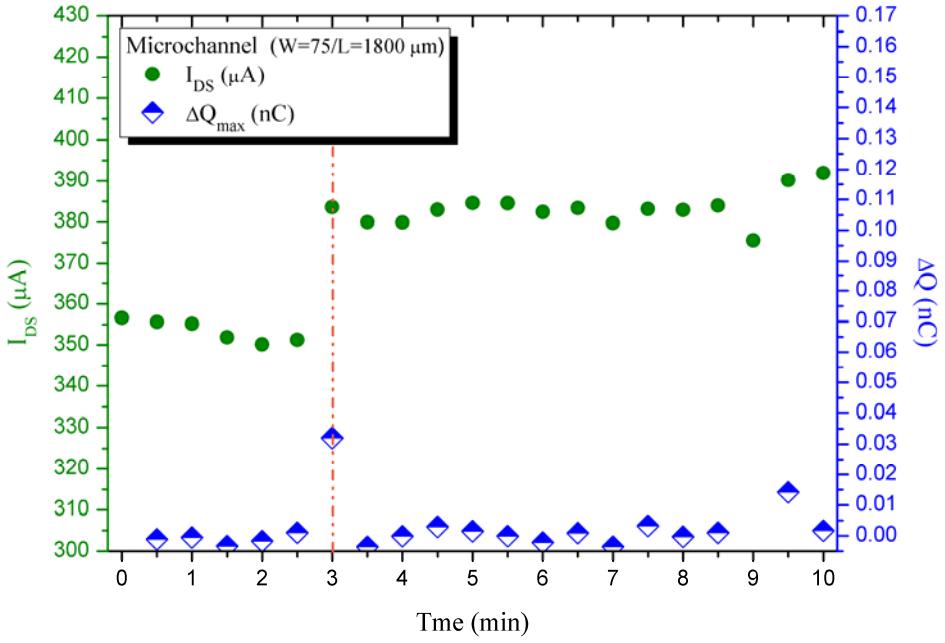

Fig 2.9 (Microfluidic channel length 1800 μm) Drain current and induced charge variation

The following diffusion equation is employed to explain the correlation of channel length and response time [26].

$$x^2 = 2\,D\,t \qquad (2.1)$$

which x is the mean length of displacement, D is the diffusion coefficient of the IgG antibody solution and t is the diffusion time. By fixing the concentration of IgG antibody solution (in this case, IgG antibody : PBS = 1:50), the diffusion coefficient D is a constant value. As a result, the mean square displacement x^2 is proportional to the diffusion time t.

In our case, with the microchannel length 1800 μm and the response time 3.0 minute, D is calcuated to be 5.4×10^5 μm^2/min. The value is close to the case of 2700 μm length and 6.5 minute response time with D = 5.6×10^5 μm^2/min. The difference may be attributed to serpentine shape of the micochannel, for the fluid flow rate in the curved region is different from that in the straight line region.

It verifies that the diffusion equation can describe our experiment. Thus, IgG antibody goes from pool to the sensing pad is a “diffusion” phenomenon.

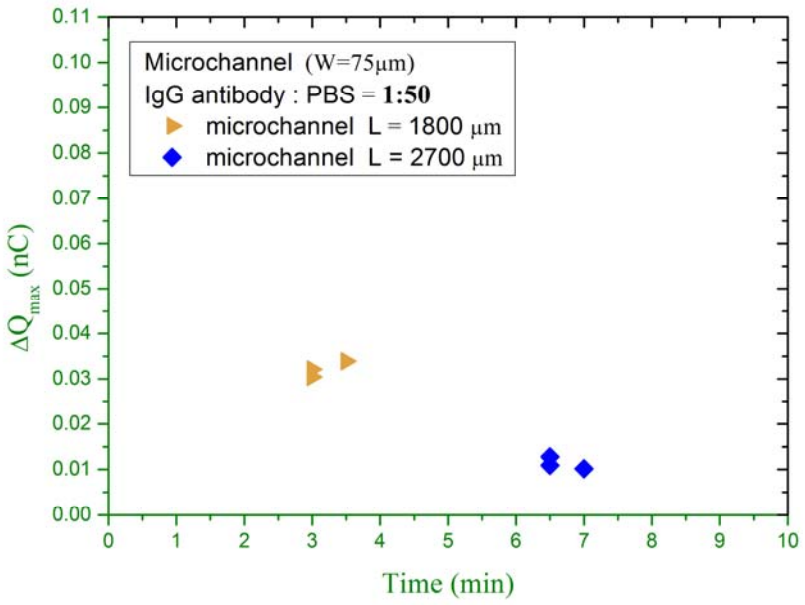

Fig 2.10 Summary of response time and $\triangle Q_{max}$ (IgG antibody : PBS= 1:50)

2.3.2 Induced charge variations in time domain

To further understand the amount of additional changes sensed by the device so that the concentration of IgG can be benchmarked. The amount of induced charges in the IGZO TFT is obtained from the following equation [27]:

$$Q = \frac{2}{3}WLC(V_G - V_T) \tag{2.2}$$

$$I_D = \frac{1}{2}\mu C\frac{W}{L}(V_G - V_T)^2 \tag{2.3}$$

which Q is the induced charge in the IGZO channel, W and L are the width and length of the TFT channel respectively, C is the insulator capacitance per unit gate area, V_{GS} is the voltage between gate and source, V_T is the threshold voltage of the transistor and μ is the mobility of carriers in the channel. By combining Equation (2.2) and (2.3), the induced charge Q is correlated only to the drain current I_D by

$$Q = \left(\frac{8}{9}\frac{WL^3C}{\mu}I_{DS}\right)^{0.5} \tag{2.4}$$

Here we define change difference at each time interval,

$$\Delta Q(t) = Q(t) - Q(t\text{-}30\ \text{sec})$$

Which Q(t) is the calculated charges at time t from Equation (2.4), and Q(t-30 sec) is the charges at the previous measurement, i.e., t-30 sec.

In Fig 2.7, as the protein reached the sensing pad, $\triangle Q_{max}$ is 0.0109nC at t = 6.5 min with the microchannel length being 2700 μm. On the other hand, for the case with the microchannel length of 1800 μm in Fig 2.9, $\triangle Q_{max}$ is 0.0321 nC at t = 3 min.

The dependence of IgG concentration on the electrical properties was next examined. Fig 2.11 and Table 2.1 are the summary of the response time and ΔQ_{max} for the samples with different microchannel lengths and various IgG antibody concentrations. With microchannel length being 2700 μm and a higher IgG concentration (IgG antibody : PBS = 1:30), the response time is earlier (t = 4 min) and ΔQ_{max} (0.0304 nC) is also larger as shown in Table 2.1.

Table 2.1 Summary of response time and $\triangle Q_{max}$

Concentration (IgG antibody : PBS)	Length = 2700 μm		Length = 1800 μm	
	Time (min)	ΔQ_{max} (nC)	Time (min)	ΔQ_{max} (nC)
1:30	4.0	0.0304	1.5	0.1048
1:50	6.5	0.0109	3.0	0.0321
1:100	8.5	0.0052	4.0	0.0175

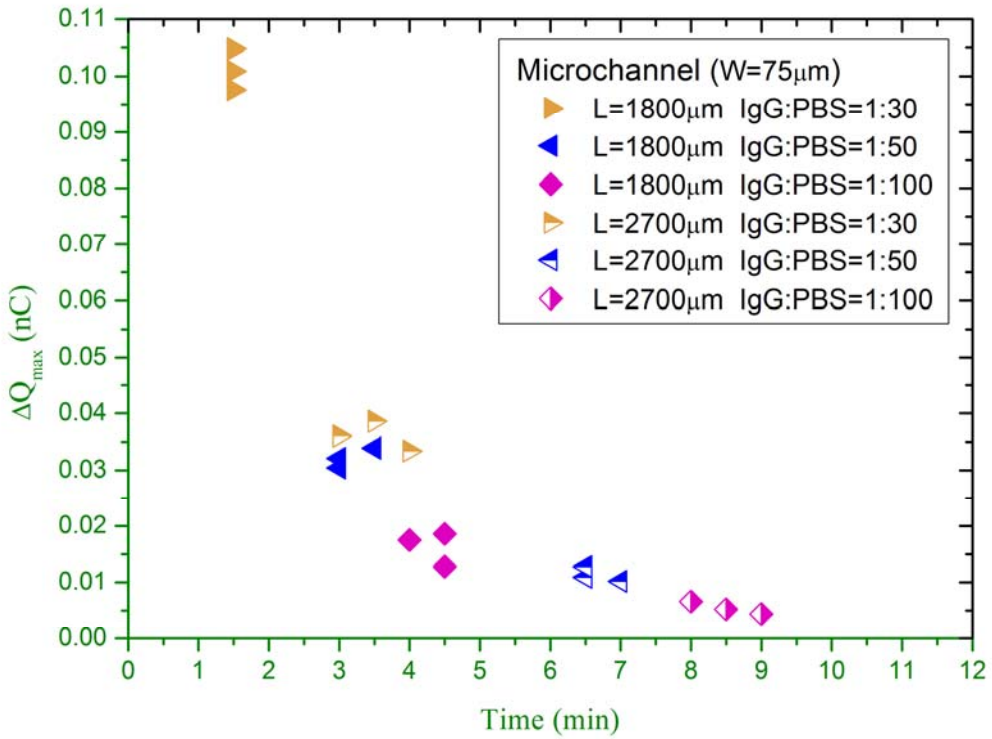

Fig 2.11 Summary of response time and $\triangle Q_{max}$

Table 2.2 lists the D calculated from Equation (2.1) with different concentration of IgG antibody solution. It indicats that with the same concentration, the diffusion coefficient is also the same.

Table 2.2 Diffusion coefficient calculated from equation (2.1)

Microchannel length	2700μm	1800μm
	Diffusion coefficient (μm^2/min)	
Antibody 1:30	11.2×10^5	10.8×10^5
Antibody 1:50	5.4×10^5	5.1×10^5
Antibody 1:100	4.2×10^5	3.83×10^5

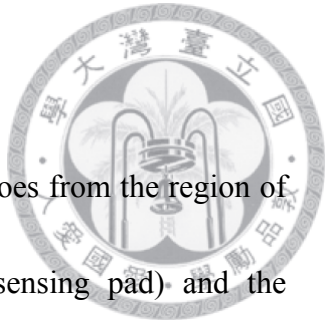

By Fick's first law of diffusion [26, 28], the diffusion flux goes from the region of high concentration (pool) to the one of low concentration (sensing pad) and the magnitude of the flux is proportional to the concentration gradient.

$$J = -D \cdot \frac{\Delta\varphi}{\Delta x} \tag{2.5}$$

φ is the concentration and x is the diffusion length. J is the diffusion flux, which means the amount of substance that flows through a cross-section during a small time interval [28]. Since ΔQ means the amount of induced charges (which are carried by IgG antibody) sense on the extended pad at a certain time. Thus, ΔQ is similar to J. D is the diffusion coefficient and is depends on temperature, viscosity of the fluid and the size of the particles according to the Stokes-Einstein relation [26]. To simplify the analysis, Equation (2.1) provides a first order estimation of the diffusion coefficient. With the same x, D is reversely proportional to diffusion time t following $D \propto \frac{1}{t}$.

Equation (2.5) can also be simplified to the following equation with a constant microchannel (diffusion) length x.

$$\Delta Q \propto \frac{\Delta\varphi}{t} \tag{2.6}$$

As the microchannel length is fixed at 2700 μm (Fig 2.12) , the value of ΔQ_{max} is 0.0109 nC with concentration of antibody is $\frac{1}{50}$. Then, evaluate the ΔQ_{max} with $\frac{1}{30}$ concentration by using relation (2.6). The $\Delta Q_{calculated}$ is 0.0295 nC ,and it is very near

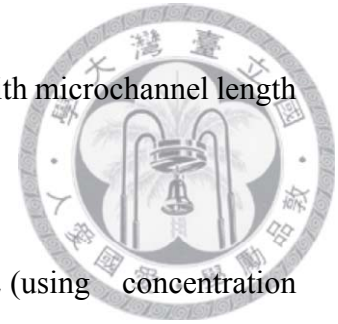

the real ΔQ_{max} which is 0.0304 nC. Fig 2.13 shows the results with microchannel length fixed at 1800 μm.

The results evaluated from relation (2.6) are listed in Table 2 (using concentration 1:50 as the standard). From the table, it is obvious that the $\Delta Q_{Calculated}$ which is evaluated from relation (2.6) are close to the ΔQ_{Real} that is measured from our device. Our experiment results fit well with the theoretical relation, which means that the concentrations of IgG antibody can be obtained by following relation (2.6).

Table 2.3 ΔQ_{Real} and $\Delta Q_{Calculated}$ from relation (2.6)

Microchannel length	Concentration of IgG antibody solution (IgG antibody : PBS)				
	1:50	1:30		1:100	
	ΔQ_{Real} (nC)	$\Delta Q_{Calculated}$ (nC)	ΔQ_{Real} (nC)	$\Delta Q_{Calculated}$ (nC)	ΔQ_{Real} (nC)
2700 μm	0.0109	0.0295	0.0304	0.0042	0.0052
1800 μm	0.0321	0.1070	0.1048	0.0120	0.0175

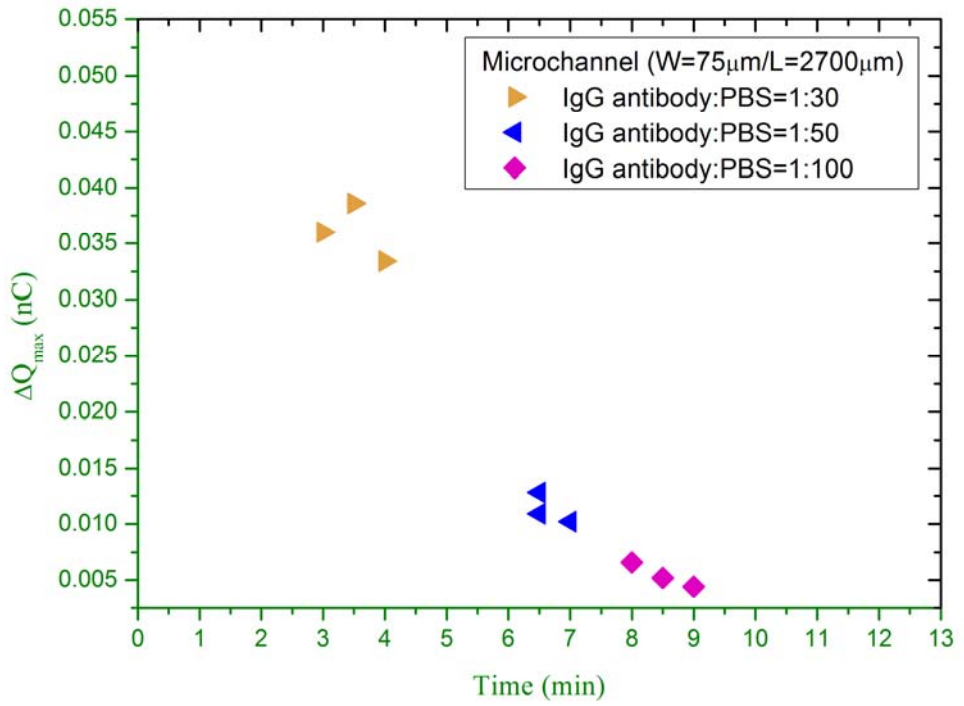

Fig 2.12 Summary of response time and △Q_{max} (2700 μm Microchannel length)

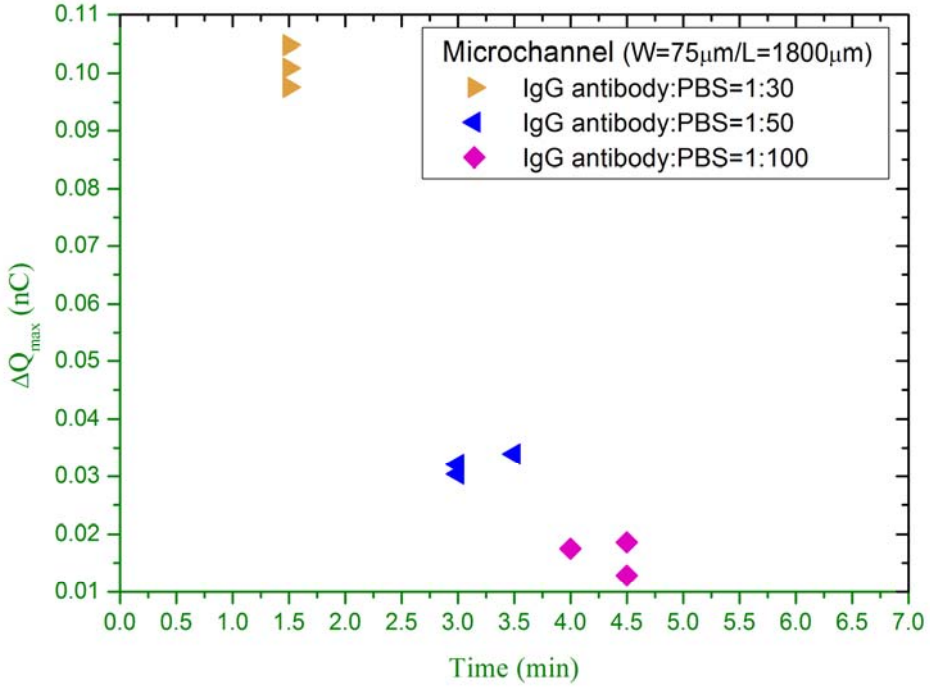

Fig 2.13 Summary of response time and △Q_{max} (1800 μm Microchannel length)

2.4 Summary

In this work, we designed a thin film transistor with extended sensing pad and microfluidic channel. Because of the concentration gradient of IgG antibody solution, the fluid diffuses to the sensing pad and creates a drain current increment.

With various microchannel length or various concentration of antibody, the results of ΔQ_{max} are quite different. All results agree well with some theoretical models, which means that the concentrations of IgG antibody can be obtained by following relation (2.6).

The response time is primarily related to the fluid condition, which depends on temperature, viscosity and the size of the particles…. etc. Another aspect, ΔQ_{max} is evaluated from drain current increment and connected with the charges carried by the biological molecules.

Comparing with the traditional FET-sensor, our design can acquire not only electrical information (i.e. the charges carried on the IgG antibody) but also fluidic information (i.e. diffusion time which is related to response time). Since microfluidic channels are often used to separate the mixture in the solution, it advantages us to divide bio-molecules and detect the charges carried on them at the same time.

In other words, if there are two different proteins in the analyte solution and both of them carried almost the same amount of charge, we can distinguish them from each other due to the different response (diffusion) time (related to protein size and weight, etc.).

Surely, our design is a convenient and simple way to identify and quantify the bio-molecules.

Chapter 3 TFT-based Biosensors and Protein-ligand Interaction

3.1 Introduction

3.1.1 Overview of Protein-ligand interaction

Finding protein-ligand binding and protein folding without external interferences is one of the most critical challenges and tasks for fundamental biological science and drug discovery, for proteins have incredible flexibilities and their proper functions in the biological systems depend on the correct folding and configurations [29, 30]. Also, protein-protein binding to form protein complexes and protein binding with small molecules provide important traces for drug discovery. Small molecules linking with proteins may produce therapeutic effects by correcting or changing the protein behaviors to activate or inactivate them. Promising drug candidates are chosen by protein-ligand binding tests among the library of millions of small molecules, typically conducted after the first screening by computer simulations [31]. However, because of the difficulties in modeling protein behaviors, the simulation often yields a very great number of drug molecule candidates for further tests. Because of the extremely high and rapidly increasing expense for drug test in the late phase of drug development, pharmaceutical companies pursue stable accurate, and high-throughput devices and methods for the screening of drug candidates in their drug discovery work flow.

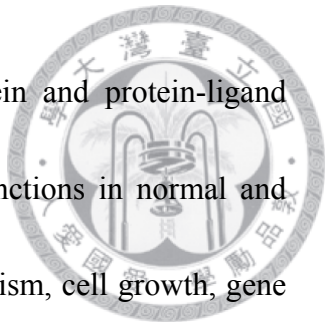

For basic biological science, uncovering the protein-protein and protein-ligand interactions is an important act to understand the biological functions in normal and diseased state[32, 33]. All biological functions including metabolism, cell growth, gene expression, enzymatic reactions, and various diseases such as immune diseases, neural diseases, cardiovascular diseases, and cancer, involve protein interactions with other proteins, small molecules, nucleic acids, ions, and other biomolecules [34]. Understanding these functions is essential to the advance of biological science. However, despite the undisputable significance of the obstacle, there has been no approach available that can detect protein interactions without interfering the analytes under test.

Most present methods involve fluorescent labeling, including the fluorescence resonance energy transfer (FRET) technique [35]. Although fluorescent tracking enables visualization of the protein molecules with excellent spatial resolution and high signal-to-noise ratio when used in fluorescence microscopy, introduction of the fluorescent components may alter the protein conditions, restrict protein folding, and affect its binding affinity or binding sites. The same issues also exist in other labeling techniques such as those with nanoparticles, quantum dots, magnetic beads, Raman probes, et cetera [36-38]. Among the label-free methods, surface plasmon resonance (SPR) is the prevailing one for protein-ligand detection. Although no labels are attached to the protein molecules in SPR assays, the ligand molecules have to be immobilized onto a solid

surface. To achieve high sensitivity and specificity, the binding sites of protein and ligand have to be very near to the gold surface of the SPR system, typically within 10 nm. This is a strict constraint on the motions of analyte proteins and their interactions with ligands. Often times in biological systems, both the proteins and the ligands are free to move in space, having high degrees of freedom to search for binding sites to form the desired configurations. However in the SPR setup, some of the degrees of freedom are taken away. Due to the lack of an interruption-free way to study protein interactions, the current techniques may yield incomplete results, either suggesting incorrect drug candidates or skipping promising ones. Thus there is a rising demand in achieving constraint-free, label-free detection of protein properties in recent years.

3.1.2 Introduction of MDH and NADH

The protein-ligand pair to be inspected in this work is chosen to be MDH and NADH.

Nicotinamide adenine dinucleotide, abbreviated NAD^+, is a coenzyme found in all living cells. The compound, possessing a molecular weight of 741.62 Da, is a dinucleotide since it consists of two nucleotides joined through their phosphate groups. One nucleotide contains an adenine base and the other nicotinamide. In metabolism, NAD^+ is involved in redox reactions, carrying electrons from one reaction to another. The coenzyme is, therefore, found in two forms in cells: NAD^+ is an oxidizing agent – it accepts electrons from other molecules and becomes reduced. This reaction forms NADH, which can then be used as a reducing agent to donate electrons.

Malate dehydrogenase (MDH) is an enzyme that reversibly catalyzes the oxidation of NADH to NAD^+ using the reduction of oxaloacetate to malate. This reaction is part of many metabolic pathways, including the citric acid cycle. According to Devenyi et al. (1966) the molecule is composed of similar subunits of molecular weight 35,000, and has a total molecular weight of 70,000 [39, 40].

3.2 Device fabrication and measurement

3.2.1 Fabrication

The fabrication process is the same as in Chapter 2. Staggered bottom-gate TFTs are fabricated on the Corning Eagle 2000 glass substrate. The process starts from molybdenum (Mo) gate metal by DC sputtering and reactive ion etching (RIE). SiO_2 dielectric layer is then deposited by plasma enhanced chemical vapor deposition (PECVD). IGZO film is coated by RF sputtering at room temperature subsequently, and the channel mesa is patterned by photolithography and dipping into dilute HCl for several seconds. Mo metal is coated by DC sputtering and etched by RIE, forming source and drain contacts. SiO_2 passivation layer is deposited by RF sputtering at room temperature for the purpose of protecting the devices and also as an insulator for the sensing metal pad. The via-holes are opened by RIE to expose the contact pads. After the fabrication of the TFT, the sensing gold pad is formed by E-gun evaporation followed by lift-off. Post-annealing at 300°C is then performed under nitrogen ambient for an hour in the oven tube. Finally, 100 μm SU-8 is coated and patterned by photolithography to be the micro-sink, or pool, and microfluidic channel of the bio-solution.

1. Gate(Mo), DC sputter , RIE etching

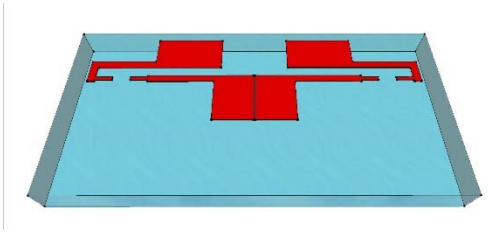

2. Insulator(SiO_2), PECVD (350℃)

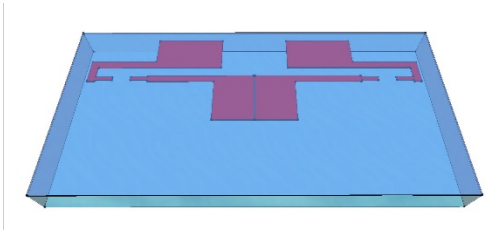

3. Channel(IGZO), RF sputter , HCl wet etching

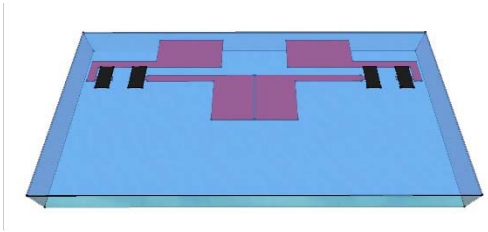

4. Source/Drain(Mo), DC sputter , RIE etching

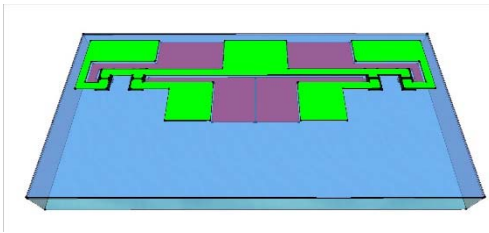

5. Passivation(SiO_2), RF sputter, RIE etching

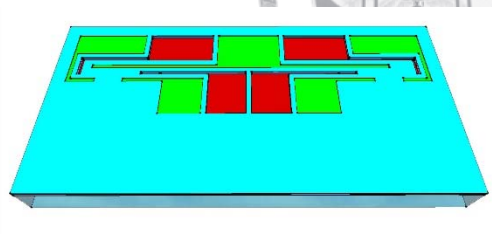

6. Sensing pad(Gold), E-Gun evaporation , Lift-off

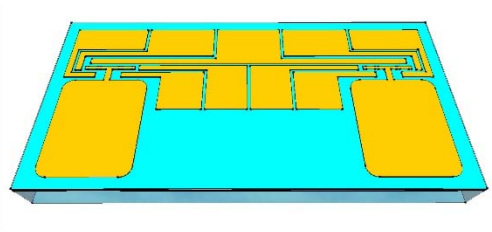

7. Microfluidic pool/channel, SU-8 photolithography

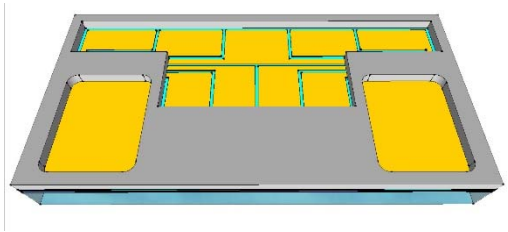

Fig 3.1. Fabrication process

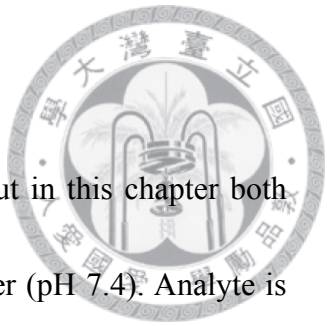

3.2.2 Method of measurement

The measurement method is similar to that in chapter 2. But in this chapter both pools and the fluidic channel are prefilled with 0.05 M Tris buffer (pH 7.4). Analyte is introduced into the left pool at t = 0 min. Drain current is sampled at V_{GS} = 8 V, V_{DS} = 5 V for 187 nM NADH every 30 seconds. As for 1.03 μM MDH, the signal is monitored under subthreshold V_{GS} region (V_{DS} still at 5 V). Current change is calculated with respect to TFT bare state (when nothing is on the sensing pad).

When conducting protein-ligand interaction measurement, both pools and the fluidic channel are prefilled with 0.05 M Tris buffer and 1.03 μM MDH. We then apply 187 nM NADH to the left pool, and start drain current sampling at V_{GS} = 8 V, V_{DS} = 5 V.

3.3 Results and Discussion

Agilent 4155C semiconductor parameter analyzer is used to extract the electrical properties of the TFTs at room temperature. The channel width and length of our IGZO TFT sensor in this chapter are 100 μm and 50 μm, respectively, with microfluidic channel being 2000 μm. We first measured the signal of our targets, i.e. NADH and MDH, separately.

In the tests of 187nM NADH diffusion, TFT drain current was measured at the bias condition V_{GS} = 8 V and V_{DS} = 5 V. The measurement was taken every 30 seconds. The drain current jump occurs at t = 4.5 ~ 5 min, with an increase percentage of 12.5% with respect to bare state, as shown in Fig. 3.2.

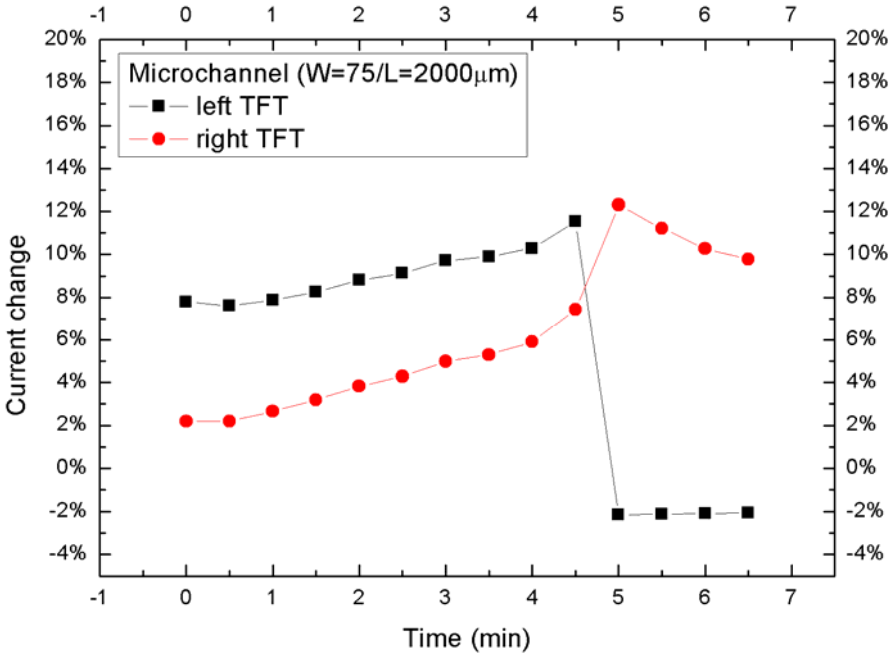

Fig 3.2. Drain current sampling of a pair of TFT sensors in a test of NADH diffusion. The lines connecting the dots are for the ease of eye-tracking.

Figure 3.3 shows the transfer curve of the device before (t = 0 min) and after (t = 5 min) sensing 187nM NADH. At V_{GS} = 8 V and V_{DS} = 5 V, the drain current is 8.30 nA at t = 0 min, and increases to 9.32 nA at t = 5 min.

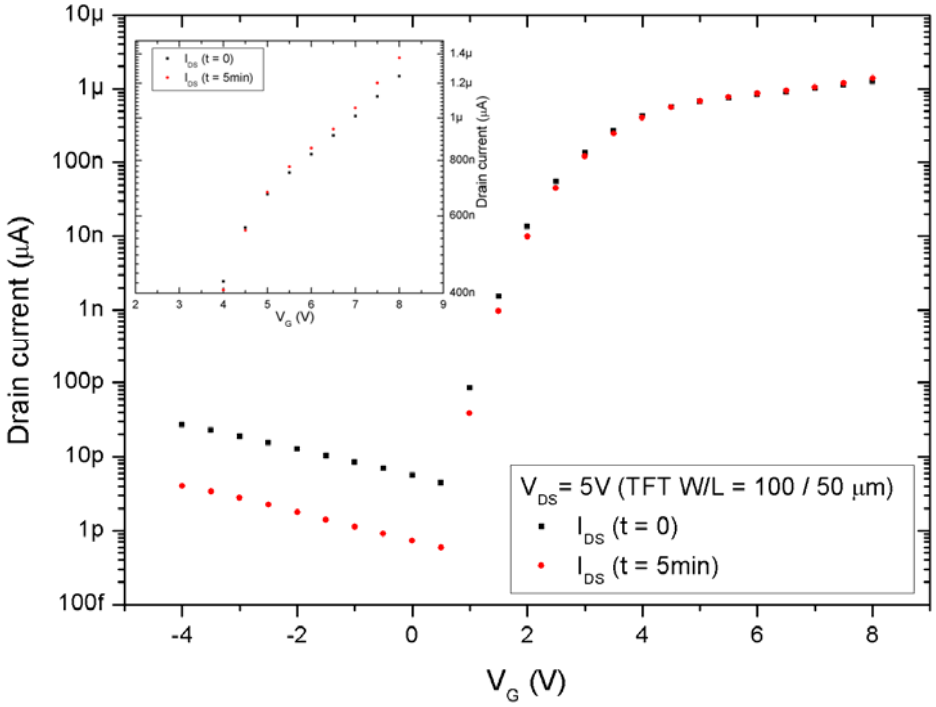

Fig 3.3. Transfer curve of a-IGZO TFT at t = 0 and 15 min. The inset shows the magnified region of V_G = 4 ~ 8 V. The drain current increased from 8.30 nA to 9.32 nA at V_G = 8 V after NADH reaches the sensing pad.

The NADH concentration of 187nM is chosen for that, under this analyte concentration, the arrival time for NADH from the introduction pool to the sensing pad is estimated to be at t = 4.0 min. The diffusion coefficient D in Eq. (2.1) can be further expressed as

$$D = \frac{1}{f}kT \tag{3.1}$$

in which k, T are Boltzman constant and absolute temperature, and f being the frictional coefficient where

$$f = 6\pi\eta r \tag{3.2}$$

For a simple estimation, we assume our targets share a similar mass density so that $f \propto r \propto V^{\frac{1}{3}} \propto M^{\frac{1}{3}}$. And from previous results summarized in Table 2.1 we can roughly say that diffusion coefficient D is proportional to $C^{1.5}$, where C is the target concentration. Following this argument we can calculate the diffusion coefficient of NADH by referring to our data in Chapter 2 as

$$D_{NADH} = D_{IgG} \times \left(\frac{C_{NADH}}{C_{IgG}}\right)^{1.5} \times \left(\frac{M_{IgG}}{M_{NADH}}\right)^{\frac{1}{3}} \tag{3.3}$$

And by Eq. (2.1), Eq. (3.3) is equal to $\frac{x^2}{2t}$. Assigning L, the microfluidic channel length, to x, Eq. (3.3) leads to

$$C_{NADH} = \left[\frac{C_{IgG}^{1.5}}{D_{IgG}} \times \left(\frac{M_{NADH}}{M_{IgG}}\right)^{\frac{1}{3}} \times \frac{L^2}{2t}\right]^{\frac{2}{3}} \tag{3.4}$$

Thus by choosing an arrival time that is suitable for our measuring condition, say, 4 minutes, we have obtained that an NADH concentration of 187nM should be used. In Fig. 3.x, the arrival time falls between t = 4.5 or 5 min, indicating that our estimation has a certain precision on predicting target arrival time to the same order of magnitude. Equation (3.4) is useful when encountering a new analyte of unknown diffusion coefficient. By choosing an acceptable range of the target arrival time, the analyte solution concentration is decided. And after testing, the diffusion coefficient of the analyte is in

turn determined.

We next measured the diffusion signal the other target, MDH, in concentration of 1.03 μM as calculated by Eq. (3.4). The drain current was sampled under V_{GS} in subthreshold region (-2 V) and V_{DS} = 5 V, with a same sampling rate of 30 seconds. At t = 10.0 min, an increase of current from 15.1 pA to 18.6 pA (see Fig 3.4) indicates the device has sensed the diffusion of MDH over to the other pool. In the meanwhile we observed that there is a current drop in the left TFT, which is related to the pool that analyte is introduced in. This one-decrease-the-other-increase observation is quite common among our experimental results, and can be reasonably interpreted as a portion of analyte leaving the pool while diffusing to the other.

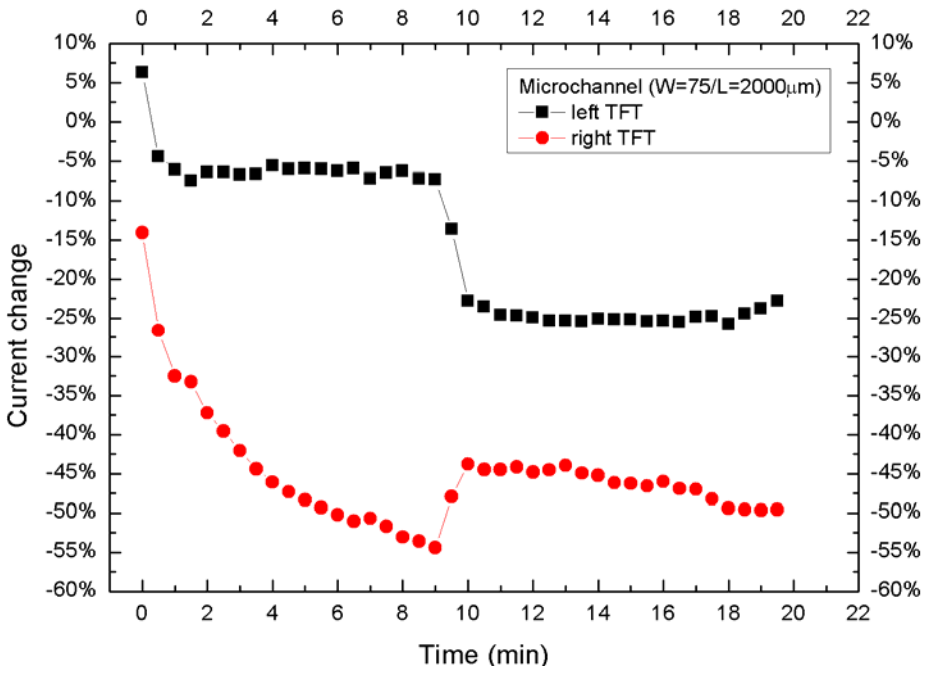

(a)

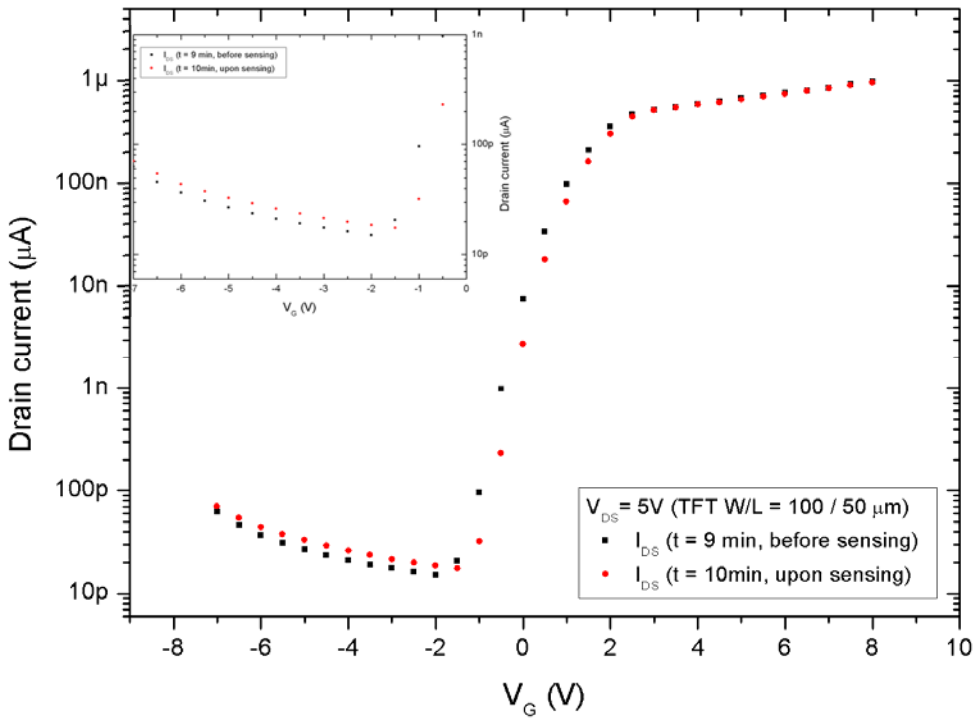

(b)

Fig 3.4. (a) Drain current sampling in time domain (b) TFT transfer curve before and after MDH sensing. The inset shows the magnified subthreshold region. The drain current increased from 15.1 pA to 18.6 pA at V_G = -2 V after MDH reaches the sensing pad.

Apart from exploiting electrical properties of our device to detect biological analyte, we also use NHS-Fluorescein, a fluorescent dye label with excitation and emission wavelength being 494 and 518 nm respectively, to verify the diffusion scheme. NHS-Fluorescein is a amine-reactive derivative of fluorescein dye that have wide-ranging application as antibody and other probe labels for use in fluorescence microscopy, flow cytometry and immunofluorescence-based assays such as Western blotting and ELISA. It

is capable of labeling MDH, our analyte, by binding onto its primary amines. We can then observe the process of diffusion under a fluorescent microscope. Figure 3.5 shows the snapshots of a complete diffusion event. We first fill both of the pools and the microfluidic channel with buffer solution. Then we apply 1.03 μM MDH to the left pool and at the same time we start taking pictures every 30 seconds. From the figure we can see that fluorescent labeled MDH steadily fill up the microfluidic channel and gradually spread out from the channel outlet onto the surface of the other pool. The fluorescent proportion became most obvious around 7.5 ~ 8.0 min, slightly quicker than that determined electrically (9.5 ~ 10 min). The emission weakens after t = 10 min because that the fluorescein eventually dies out. These fluorescent snapshots give a hint that it requires a certain amount of analyte for the device to trigger a sensing response. A few minutes ahead of electrically determined arrival time, we see that there are already some fluorescein sparkling around the channel outlet. This implies in this case the time it takes for analyte to diffuse through the microfluidic channel is actually shorter than we measured previously. But not until enough amount of analyte has diffused onto the sensing pad does it cross over the detection limit of our device to make a response.

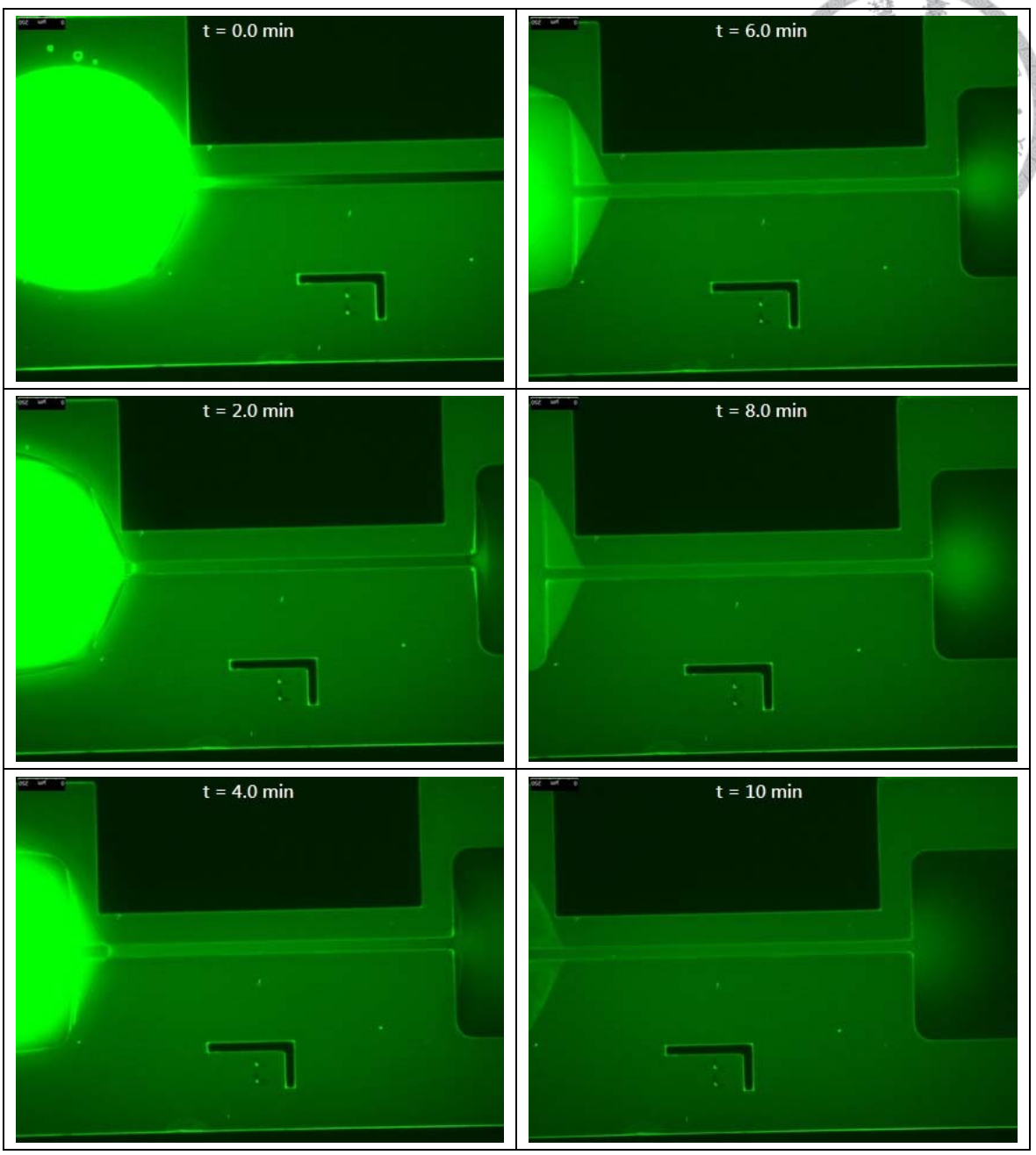

Fig 3.5. Snapshots of the diffusion process of NHS-fluorescent-binding MDH. The pictures were taken every 30 seconds (others not shown).

Finally we conduct the mixing diffusion experiment to examine the signal of protein-ligand interaction. We fill both of the pools with 1.03 μM MDH and 0.05 M Tris buffer. 187 nM NADH is then introduced into the left pool. Drain current variation in time domain is shown in Fig. 3.6. A sudden current increase at t = 5 ~ 6 min is observed and is considered the signal of the arrival of NADH to the right-hand-side sensing pad, since the arrival time and current gain percentage (10.1%) is matching our previous experimental results on separate target detection (t = 5 min, gain 12.5%).

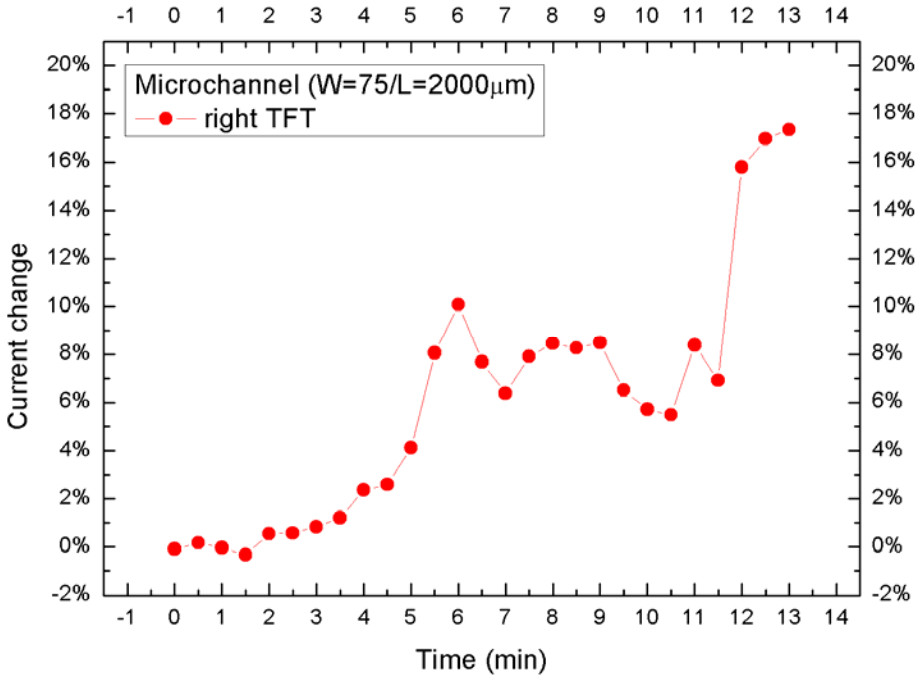

Fig 3.6. Drain current variation of mixing analyte diffusion in time domain. The signal of the left-hand-side sensor is hidden to avoid distraction.

A second current jump is observed at t = 12 min. This sudden increase is considered to be the outcome of the chemical reaction below,

$$NADH + H^+ + oxaloacetate \overset{MDH}{\Longleftrightarrow} NAD^+ + L - malate \quad (3.5)$$

Research shows that NADH acts as an electron donor in many other biological-related chemical reactions. Upon applying to the pool, NADH sets out to the other side due to concentration gradient. After reaching the sensing pad, NADH participate in the chemical reaction of Eq. (3.5) catalyzed by MDH, donating its electron and turning into the oxidized form of NAD^+. The election transfer of the oxidation may lead to a change in local charge distribution near the sensing pad [41], causing the second current jump in time domain.

Another possible explanation could be the diffusion signal of the product of the redox reaction. After the introduction of NADH, L-malate is formed in the left pool. Thus a concentration gradient of L-malate is created across the microfluidic channel, causing it to diffuse through the fluidic channel and induce the second current gain. According to Eq. (3.4), a diffusion time of 12 min, the time interval between the addition of NADH and the second current jump, implies an analyte with a concentration of 61.5 nM has diffused to the other sensing pad. Following this calculation we can further deduce that 32.9% of NADH in the initial introduction is consumed during the redox reaction in the left pool.

3.4 Summary

In this work, we put further application to our TFT biosensor as to detect the chemical reaction of our analytes.

First we measure the diffusion and electrical signals of our targets separately. We deduced Eq. (3.4) to estimate a desirable diffusion arrival time. The experimental results proved that the time estimation is accurate down to the same order of magnitude. Therefore Eq. (3.4) is useful when encountering a new analyte, for it can be applied to determine appropriate experimental concentration and thus determining the diffusion coefficient of the new analyte.

A series of fluorescent snapshots have been taken to reveal the complete diffusion scheme of our target molecule through the microfluidic channel. The snapshots provide a visual verification of our measurement results, which mainly relies on electrical signals. We find that NHS-fluorescein-binding MDH appears a few minutes ahead of our electrically detected arrival time. This could mean that there exists a sensing threshold in our device. A certain amount of analyte has to be diffused onto the sensing pad to be detected by our device.

The chemical reaction of MDH and NADH is examined by the mixing diffusion experiment. Besides the arrival signal of NADH as observed in previous tests, the signal of NADH oxidation is detected as well.

Chapter 4 Conclusion

4.1 TFT-based biosensors with microfluidic channels

In chapter 2, we demonstrated a TFT-based biosensor with extended sensing metal pad and microfluidic channel. Due to the created concentration gradient of IgG antibody solution, the analyte solution diffuses to the sensing pad and creates a drain current increment.

As the microchannel length and concentration of antibody are different, the results of response time and ΔQ_{max} are quite distinguishable. All results agree well with some theoretical models, which means that the concentrations of IgG antibody can be obtained.

The response time is mainly related to the fluid condition. In the meanwhile, ΔQ_{max} is evaluated from drain current increment and connected with the charges carried by the biological molecules. Thus, our design can acquire both fluidic (protein size and weight) and electrical (charge carried on protein) information at the same time.

4.2 TFT-based biosensors and protein-ligand interaction

In chapter 3, we examine the diffusion and electrical signals of protein, ligand, and protein-ligand interaction. Our analyte are chosen to be MDH and NADH. They were first measured separately to obtain information that would be referenced for later experiment.

An estimation equation is provided for new analyte with unknown diffusion coefficient, and is verified in our experiment to have accurate evaluation of diffusion time. We also did the fluorescent snapshots to gain a visual picture of the diffusion scheme aside from electrical measurement.

Finally, the protein-ligand interaction is detected by our TFT sensor. The electron transfer of the oxidation of NADH into NAD^+ is reflected in the second current jump in time domain.

References

[1] D.-S. Kim, J.-E. Park, J.-K. Shin, P. K. Kim, G. Lim, and S. Shoji, "An extended gate FET-based biosensor integrated with a Si microfluidic channel for detection of protein complexes," *Sensors and Actuators B: Chemical,* vol. 117, pp. 488-494, 2006.

[2] P. O. Brown and D. Botstein, "Exploring the new world of the genome with DNA microarrays," *Nature genetics,* vol. 21, pp. 33-37, 1999.

[3] K. E. Nelson, L. Gamble, L. S. Jung, M. S. Boeckl, E. Naeemi, S. L. Golledge*, et al.*, "Surface characterization of mixed self-assembled monolayers designed for streptavidin immobilization," *Langmuir,* vol. 17, pp. 2807-2816, 2001.

[4] P. I. Reyes, C.-J. Ku, Z. Duan, Y. Lu, A. Solanki, and K.-B. Lee, "ZnO thin film transistor immunosensor with high sensitivity and selectivity," *Applied Physics Letters,* vol. 98, p. 173702, 2011.

[5] C. V. Sapan, R. L. Lundblad, and N. C. Price, "Colorimetric protein assay techniques," *Biotechnology and applied Biochemistry,* vol. 29, pp. 99-108, 1999.

[6] R. L. Ashley, J. Militoni, F. Lee, A. Nahmias, and L. Corey, "Comparison of Western blot (immunoblot) and glycoprotein G-specific immunodot enzyme assay for detecting antibodies to herpes simplex virus types 1 and 2 in human sera," *Journal of Clinical Microbiology,* vol. 26, pp. 662-667, 1988.

[7] M. S. Smeltzer, M. E. Hart, and J. J. Iandolo, "Quantitative spectrophotometric assay for staphylococcal lipase," *Applied and environmental microbiology,* vol. 58, pp. 2815-2819, 1992.

[8] E. Stenberg, B. Persson, H. Roos, and C. Urbaniczky, "Quantitative determination of surface concentration of protein with surface plasmon resonance using radiolabeled proteins," *Journal of colloid and interface science,* vol. 143, pp. 513-526, 1991.

[9] B.-K. Sohn and C.-S. Kim, "A new pH-ISFET based dissolved oxygen sensor by employing electrolysis of oxygen," *Sensors and Actuators B: Chemical,* vol. 34, pp. 435-440, 1996.

[10] S. V. Dzyadevich, Y. I. Korpan, V. N. Arkhipova, M. Y. Alesina, C. Martelet, A. V. El'Skaya*, et al.*, "Application of enzyme field-effect transistors for determination of glucose concentrations in blood serum," *Biosensors and bioelectronics,* vol. 14, pp. 283-287, 1999.

[11] B. L. Allen, P. D. Kichambare, and A. Star, "Carbon Nanotube Field-Effect-Transistor-Based Biosensors," *Advanced Materials,* vol. 19, pp. 1439-1451, 2007.

[12] I. Lauks, P. Chan, and D. Babic, "The extended gate chemically sensitive field effect transistor as multi-species microprobe," *Sensors and Actuators,* vol. 4, pp. 291-298, 1983.

[13] L.-T. Yin, J.-C. Chou, W.-Y. Chung, T.-P. Sun, and S.-K. Hsiung, "Study of indium tin oxide thin film for separative extended gate ISFET," *Materials Chemistry and Physics,* vol. 70, pp. 12-16, 2001.

[14] J.-C. Chen, J.-C. Chou, T.-P. Sun, and S.-K. Hsiung, "Portable urea biosensor based on the extended-gate field effect transistor," *Sensors and Actuators B: Chemical,* vol. 91, pp. 180-186, 2003.

[15] A. Manz, N. Graber, and H. Widmer, "Miniaturized total chemical analysis systems: a novel concept for chemical sensing," *Sensors and actuators B: Chemical,* vol. 1, pp. 244-248, 1990.

[16] S. Sharma, K. Buchholz, S. M. Luber, U. Rant, M. Tornow, and G. Abstreiter, "Silicon-on-insulator microfluidic device with monolithic sensor integration for μTAS applications," *Microelectromechanical Systems, Journal of,* vol. 15, pp. 308-313, 2006.

[17] S. C. Jacobson, R. Hergenroder, L. B. Koutny, and J. M. Ramsey, "High-speed separations on a microchip," *Analytical Chemistry,* vol. 66, pp. 1114-1118, 1994.

[18] M. Szumski and B. Buszewski, "State of the art in miniaturized separation techniques," *Critical reviews in analytical chemistry,* vol. 32, pp. 1-46, 2002.

[19] S. C. Jakeway, A. J. de Mello, and E. L. Russell, "Miniaturized total analysis systems for biological analysis," *Fresenius' journal of analytical chemistry,* vol. 366, pp. 525-539, 2000.

[20] P.-A. Auroux, D. Iossifidis, D. R. Reyes, and A. Manz, "Micro total analysis systems. 2. Analytical standard operations and applications," *Analytical chemistry,* vol. 74, pp. 2637-2652, 2002.

[21] D. Erickson and D. Li, "Integrated microfluidic devices," *Analytica Chimica Acta,* vol. 507, pp. 11-26, 2004.

[22] M. J. de Boer, R. W. Tjerkstra, J. Berenschot, H. V. Jansen, G. Burger, J. Gardeniers, *et al.*, "Micromachining of buried micro channels in silicon," *Microelectromechanical Systems, Journal of,* vol. 9, pp. 94-103, 2000.

[23] L.-M. Fu, R.-J. Yang, C.-H. Lin, Y.-J. Pan, and G.-B. Lee, "Electrokinetically driven micro flow cytometers with integrated fiber optics for on-line cell/particle detection," *Analytica Chimica Acta,* vol. 507, pp. 163-169, 2004.

[24] K. Hatakeyama, T. Tanaka, M. Sawaguchi, A. Iwadate, Y. Mizutani, K. Sasaki, *et al.*, "Microfluidic device using chemiluminescence and a DNA-arrayed thin film transistor photosensor for single nucleotide polymorphism genotyping of PCR amplicons from whole blood," *Lab on a Chip,* vol. 9, pp. 1052-1058, 2009.

[25] C. A. Janeway, P. Travers, M. Walport, and M. J. Shlomchik, "The structure of a typical antibody molecule," 2001.

[26] 鄭. Reist, 劉希平, "微粒導論," ed: 國立編譯館, 2001.

[27] P. J. H. P.G. Gray, S.H. Lewis , R.G. Meyer, *Analysis and Design of Analog Integrated circuit, 4th edition*: John Wiley & Sons ,Inc., 2001.

[28] W. F. Smith, *Foundations of Materials Science and Engineering 3rd ed.*: McGraw-Hill, 2004.

[29] J. C. Young, V. R. Agashe, K. Siegers, and F. U. Hartl, "Pathways of chaperone-mediated protein folding in the cytosol," *Nature reviews Molecular cell biology,* vol. 5, pp. 781-791, 2004.

[30] K. A. Dill, "Dominant forces in protein folding," *Biochemistry,* vol. 29, pp. 7133-7155, 1990.

[31] A. C. Wallace, R. A. Laskowski, and J. M. Thornton, "LIGPLOT: a program to generate schematic diagrams of protein-ligand interactions," *Protein engineering,* vol. 8, pp. 127-134, 1995.

[32] A. Ho and T. C. Südhof, "Binding of F-spondin to amyloid-β precursor protein: a candidate amyloid-β precursor protein ligand that modulates amyloid-β precursor protein cleavage," *Proceedings of the National Academy of Sciences of the United States of America,* vol. 101, pp. 2548-2553, 2004.

[33] U. Francke, M. S. Brown, and J. L. Goldstein, "Assignment of the human gene for the low density lipoprotein receptor to chromosome 19: synteny of a receptor, a ligand, and a genetic disease," *Proceedings of the National Academy of Sciences,* vol. 81, pp. 2826-2830, 1984.

[34] G. Jones, P. Willett, and R. C. Glen, "Molecular recognition of receptor sites using a genetic algorithm with a description of desolvation," *Journal of molecular biology,* vol. 245, pp. 43-53, 1995.

[35] R. B. Sekar and A. Periasamy, "Fluorescence resonance energy transfer (FRET) microscopy imaging of live cell protein localizations," *The Journal of cell biology,* vol. 160, pp. 629-633, 2003.

[36] I. L. Medintz, H. T. Uyeda, E. R. Goldman, and H. Mattoussi, "Quantum dot bioconjugates for imaging, labelling and sensing," *Nature materials,* vol. 4, pp. 435-446, 2005.

[37] Q. A. Pankhurst, J. Connolly, S. Jones, and J. Dobson, "Applications of magnetic nanoparticles in biomedicine," *Journal of physics D: Applied physics,* vol. 36, p. R167, 2003.

[38] Y. C. Cao, R. Jin, J.-M. Nam, C. S. Thaxton, and C. A. Mirkin, "Raman dye-labeled nanoparticle probes for proteins," *Journal of the American Chemical Society,* vol. 125, pp. 14676-14677, 2003.

[39] J. Holbrook and R. Wolfe, "Malate dehydrogenase. X. Fluorescence microtitration studies of D-malate, hydroxymalonate, nicotinamide dinucleotide, and dihydronicotinamide-adenine dinucleotide binding by mitochondrial and supernatant porcine heart enzymes," *Biochemistry,* vol. 11, pp. 2499-2502, 1972.

[40] C. Thorne, L. Grossman, and N. Kaplan, "Starch-gel electrophoresis of malate dehydrogenase," *Biochimica et Biophysica Acta (BBA)-Specialized Section on Enzymological Subjects,* vol. 73, pp. 193-203, 1963.

[41] Y. R. Gokarn, R. M. Fesinmeyer, A. Saluja, V. Razinkov, S. F. Chase, T. M. Laue, *et al.*, "Effective charge measurements reveal selective and preferential accumulation of anions, but not cations, at the protein surface in dilute salt solutions," *Protein Science,* vol. 20, pp. 580-587, 2011.